Electronic Supplementary Material (ESI) for Dalton Transactions.
This journal is © The Royal Society of Chemistry 2023

Supporting Information for

Magnetic properties in two coordination isomeric cobalt(II) single-ion magnets

Hui-Hui Cui,*[a] Hong-Juan Xu,[a] Tengkun Zhang,[a] Shuchang Luo,*[b] Wei Tong,[c] Miao Wang,[a] Jin Wang,[a] Lei Chen,[d] Yanfeng Tang*[a]

[a]*School of Chemistry and Chemical Engineering, Nantong University, Jiangsu 226019, P. R. China.*

[b]*School of Chemical Engineering, Guizhou University of Engineering Science, Bijie, 551700, China.*

[c]*Anhui Province Key Laboratory of Condensed Matter Physics at Extreme Conditions, High Magnetic Field Laboratory of the Chinese Academy of Science, Hefei 230031, Anhui, China*

[d]*School of Environmental and Chemical Engineering, Jiangsu University of Science and Technology, Zhenjiang 212003, P. R. China*

Table S1. Summary of six- and seven-coordinate Co(II)-SIMs with N_2O_4 and N_3O_4 donor sets.

compound	Donor set	coordinated geometry	τ	D/cm^{-1}	E/D	H_{dc}/Oe	U_{eff}/ cm^{-1}	Ref
$[(L1)_4Co_3(H_2O)_2](NO_3)_4\cdot CH_3OH\cdot 5H_2O$	N_2O_4	octahedron	0.724	20.8(7)	0	1000	/	S1
$[(L2)_4Co_3(H_2O)_2](NO_3)_4\cdot 6H_2O$	N_2O_4	octahedron	1.083	29.8(8)	0.02	1000	5.46	S1
$Co^{II}Y^{III}(L3)(DBM)_3$	N_2O_4	octahedron	1.923	10.3	0	2000	5.95	S2
$Co(9Accm)_2(py)_2$	N_2O_4	octahedron	0.203	74.1	0.01	1500	/	S3
$Co(9Accm)_2(2,2'\text{-bpy})$	N_2O_4	octahedron	0.761	24.1	-0.07	700	/	S3
$Co(3,5\text{-dnb})_2(py)_2(H_2O)_2$	N_2O_4	octahedron	0.169	58	0	1000	19.5	S4
$Co(3,5\text{-dnb})_2(py)_2(H_2O)_2$	N_2O_4	octahedron	0.088	68	0.22	1000	21.1	S4
$Co(H_2O)_2(CH_3COO)_2(C_5H_5N)_2$	N_2O_4	octahedron	0.072	/	/	1500	25	S5
$[Co(pydm)_2](dnbz)_2$	N_2O_4	octahedron	4.304	-94.8[a]	0.12	2000	39	S6
$[Co(pydca)(dmpy)]_2\cdot H_2O$	N_2O_4	octahedron	4.504 5.162	55	0.34	4000	/	S7
$Co(1\text{-napH})_2(4,4'\text{-bpy})_2(H_2O)_2$	N_2O_4	octahedron	0.122	|89.5|	0	1500	21.26	S8
$Co(neo)(piv)_2$	N_2O_4	octahedron	7.650	/	/	1000	13.20	S9
$[Co(neo)(4OH\text{-benz})_2]\cdot 2CH_3OH$	N_2O_4	octahedron	6.352	/	/	1000	12.16	S9
$Co(H_2DPA)_2\cdot H_2O$	N_2O_4	octahedron	2.918	67.63	-0.24	1500	30.08	S10
$[Co(hfa)_2(pic)_2]$	N_2O_4	octahedron	0.694	24.17	0.285	2000	17.38	S11
$[Co(\mu\text{-}L4)(\mu CCl_3COO)Y(NO_3)_2]\cdot 2CHCl_3\cdot CH_3CN\cdot 2H_2O$	N_2O_4	octahedron	0.758	91.37	0.25	1200	5.88	S12
$[Co(\mu\text{-}L4)(\mu\text{-}CH_3COO)Y(NO_3)_2]\cdot CH_3CN$	N_2O_4	octahedron	0.763	87.9	0.132	1200	7.65	S12
$[Co(\mu\text{-}L4)(\mu PhCOO)Y(NO_3)_2]\cdot 3CH_3CN\cdot 2H_2O$	N_2O_4	octahedron	0.800	90.02	0.206	1200	9.52	S12
$[Co(\mu\text{-}L4)\text{-}(\mu tBuCOO)Y(NO_3)_2]\cdot CHCl_3\cdot 2H_2O$	N_2O_4	octahedron	0.859	72.42	0.253	1200	12.99	S12
$[Co(hfac)_2L5]\cdot CH_3CN$	N_2O_4	octahedron	0.507	/	/	1000	5.8	S13
$[Co(pydm)_2](mdnbz)_2$	N_2O_4	octahedron	3.200	50	0.204	2500	/	S14
$[Co(hfac)_2(MeCN)_2]$	N_2O_4	octahedron	0.062	64.46	0.036	1000	8.8	S15
$[Co(hfac)_2(Spy)_2]$	N_2O_4	octahedron	0.051	59.78	0.030	1400	14.5	S15
$[Co(hfac)_2(MBIm)_2]$	N_2O_4	octahedron	0.096	67.65	-0.034	1000	16.7	S15
$[Co(L6)_2(H_2O)_2]$	N_2O_4	octahedron	0.312	-28.78	-0.281	800	30.37	S16
$[Co(HL7)_2](ClO_4)_2\cdot 2H_2O$	N_2O_4	octahedron	2.491	-23.8	-0.294	800	13.7	S17
$[Co(2,6\text{-dfba})_2(bpp)_2(H_2O)_2]_n$	N_2O_4	octahedron	0.025/ 0.076	53.19	0.144	2000	19.8	S18

$[Co(2,6\text{-dfba})_2(bpe)_2(H_2O)_2]_n$	N_2O_4	octahedron	0.117	65.67	0.068	2000	15.4	S18
$[Co(neo)(ac)_2]$	N_2O_4	trigonal prism	3.761	/	/	1000	26.201	S9
$[CoL8_2(H_2O)_2]\cdot 2H_2O\cdot 2CH_3OH$	N_2O_4	trigonal antiprism	/	/	/	1500	38.25	S19
$[CoL8_2(CH_3CH_2O)_2]$	N_2O_4	trigonal antiprism	/	/	/	600	37.56	S19

a: The ZFS parameters were obtained from the theoretical calculation.

L1 = 4-imidazocarboxylate-2-pyrazine carbohydrozone; L2 = pyridine-2-carboxylate-2-pyrazine carbohydrozone; H_2L3 = N,N'-dimethyl-N,N'-(2-hydroxy-3-methoxy-5-methyl-benzyl)ethylenediamine; DBM^- = anion of 1,3-Diphenyl-propane-1,3-dione; 9Accm = 1,7-(di-9-anthracene-1,6-heptadiene-3,5-dione); 3,5-Hdnb = 3,5-dinitrobenzoic acid; py = pyridine; Pydm = 2,6-pyridinedimethanol; dnbz = dinitrobenzoato; pydca = pyridine-2,6-dicarboxylato; dmpy = 2,6-dimethanolpyridine; $napH_2$ = 1-naphthalene phosphonic acid; 4,4'-bpy = 4,4'-bipyridine; neo = neocuproine; ac = acetate; piv = pivalate; 4OH-benz = 4-hydroxybenzoate; H_2DPA = 2,6-pyridine-dicarboxylic acid; Hhfa =1,1,1,5,5,5-hexafluoro-2,4-pentanedione; pic = 4-methylpyridine; $L4H_2$ = $Fe[(C_5H_4)\{\text{-}C(Me)=N-N=CH\text{-}C_6H_3\text{-}2\text{-}OH\text{-}3\text{-}OCH_3\}]_2$; L5 = N3,N6-bis(pyridin-2-ylmethyl)-1,2,4,5-tetrazine-3,6-diamine; Hhfac = hexafluoroacetylacetone; Pydm = 2,6-pyridinedimethanol; dnbz = dinitrobenzoato; Spy = 4-styrylpyridine; MbIm = 5,6-dimethylbenzimidazole; L6 = (E)-2-(((4H-1,2,4-triazol-4-yl)imino)methyl)-6-methoxyphenol; L7 = N'-(2-hydroxybenzylidene)acetohydrazide; 2,6-Hdfba = 2,6-difluorobenzoic acid, bpp = 1,3-bis(4-pyridyl)propane, bpe = 1,2-bis(4-pyridyl)ethylene); HL8 = quinoline-2-carboxylic acid

compound	Donor set	coordinated geometry	τ	D/cm^{-1}	E/D	H_{dc}/Oe	U_{eff}/ cm^{-1}	Ref
$[Co^{II}(H_2dapb)(H_2O)(NO_3)](NO_3)$	N_3O_4	pentagonal bipyramid	0.417	32.4	0	1000	56.3	S20
$[Co(DAPBH)(NO_3)(H_2O)](NO_3)$	N_3O_4	pentagonal bipyramid	0.417	31.0	0	1000	34.75	S21/ S22
$[Co(L9)_3(NO_3)_2]$	N_3O_4	pentagonal bipyramid	1.410	35.8	0	1000	17.7	S23
$[Co(L10)_3(NO_3)_2]$	N_3O_4	pentagonal bipyramid	1.542	35.7	0	1200	11.0	S23
$[Co^{II}(pypzbeyz)(NO_3)_2]$	N_3O_4	pentagonal bipyramid	3.010	29.9	0.01	1000	34.6	S24
$[Co(bpy)(NO_3)_2(CH_3CN)]$	N_3O_4	pentagonal bipyramid	1.89	32.9	0	1000	39.4	S25
$[Co(phen)(NO_3)_2(CH_3CN)]$	N_3O_4	pentagonal bipyramid	1.93	31.4	0	1000	32.0	S25
$[Co(H_2daps)(MeOH)_2]$	N_3O_4	pentagonal bipyramid	0.235	43.1	0.07	1000	23.28	S26
$[Co^{II}L11]\cdot H_2O$	N_3O_4	pentagonal bipyramid	3.076	29.1	0	1000	/	S27
$[Co(H_2dapsc)(H_2O)_2)](NO_3)_2\cdot 2H_2O$	N_3O_4	pentagonal bipyramid	0.191	38.02	0.018	1200	/	S28
$[Co(H_4L12)(DMF)(H_2O)](NO_3)_2\cdot(DMF)$	N_3O_4	pentagonal bipyramid	0.293	35.92	0.04	3500	17.37	S29
$[Co(H_4L12)(MeOH)(H_2O)](NO_3)_2\cdot(MeOH)$	N_3O_4	pentagonal bipyramid	0.067	37.23	0.02	3500	10.42	S29
$[Co(H_4L12)(DEF)(H_2O)](NO_3)_2$	N_3O_4	pentagonal bipyramid	0.253	43.76	0.01	3500	2.78	S29
$[Co(L13)_2(CH_3OH)_2]$	N_3O_4	pentagonal bipyramid	0.614	46.74	0.01	3000	9.20	S30

H_2dapb = 2,6-diacetylpyridine bis(benzoylhydrazine; DAPBH = 2,6-diacetylpyridinebis(2'-pyridylhydrazone); L9 = 4-tert-butylpyridine; L10 = isoquinoline; Pypzbeyz = N-((6-(1H-pyrazol-1-yl)pyridin-2-yl)methylene)benzohydrazide; bpy = 2,2'-bipyridine; phen = 1,10-phenanthroline; H_4daps = 2,6-bis(1-salicyloylhydrazonoethyl); H_2L11 = 3,12,18-triaza-6,9-dioxabicyclo[12.3.1]octadeca-1,14,16-triene-3,12-diacetic acid; H_2dapsc = 2,6-diacetylpyridine bis(semicarbazone); H_4L12 = 2,2'-(pyridine-2,6-diylbis(ethan-1-yl-1-ylidene))bis(N-phenylhydrazinecarboxamide; HL13 = 2,6-bis(pyrazole-1-yl)pyridine-4-carboxylic acid

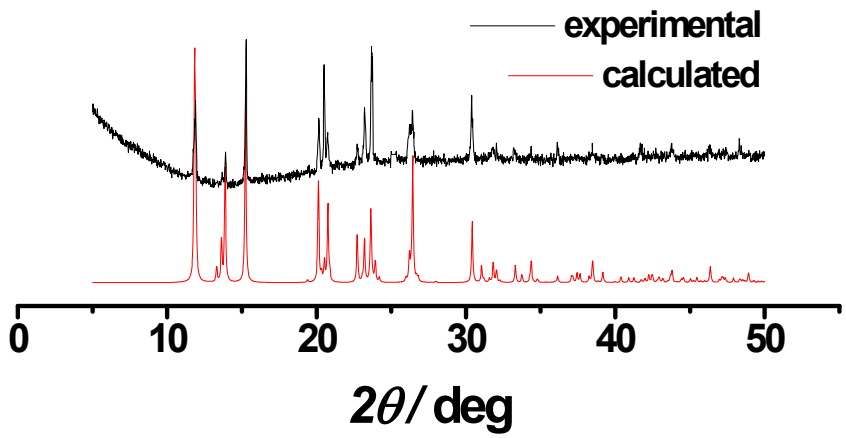

Fig. S1 XRD patterns for complex **1**.

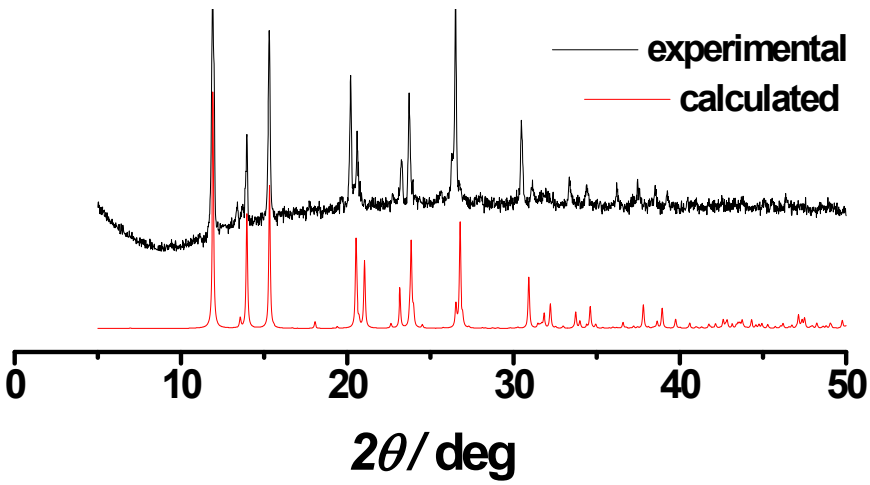

Fig. S2 XRD patterns for complex **2**.

Table S2. Summary of crystal data and refinement for **1**-**2**.

	1	**2**
Molecular formula	$C_{16}H_{12}CoN_6O_6$	$C_{16}H_{12}CoN_6O_6$
CCDC no	2226213	2226214
Formula weight	443.25	443.25
Temperature	296(2) K	296(2) K
Crystal system	Monoclinic	Monoclinic
Space group	*C*2/c	$P2_1$/c
a / Å	14.7033(7)	14.509(3)
b / Å	9.1448 (4)	9.1423(18)
c / Å	15.3254(8)	14.924(3)
α (°)	90	90
β (°)	119.853(2)	119.08
γ (°)	90	90
V / Å^3	1787.20(15)	1729.9(6)
Z	4	4
D_{calc}, g/cm^3	1.647	1.702
μ / mm^{-1}	1.010	1.044
F (000)	900	900
θ range [°]	2.741/27.672	1.606/25.265
Reflns collected	13966	12477
R_{int}	0.0254	0.0374
Indep. reflns	2086	3078
Data/restr./paras	2086/0/132	3078/3/262
Goodness-of-fit on F^2	1.190	1.049
R_1, wR_2 [I > 2σ(*I*)][a]	0.0480/0.1348	0.0249/0.0650
R_1, wR_2 [all data][a]	0.0615/0.1632	0.0307/0.0679

[a]$wR_2 = [\Sigma[w(F_o^2–F_c^2)^2]/\Sigma[w(Fo^2)^2]]^{1/2}$, $R_1 = \Sigma||F_o|–|F_c||/\Sigma|F_o|$.

Table S3. Selected bond lengths (Å) and angles (deg) for **1** and **2**.

1		**2**	
Co1-O1	2.205(2)	Co1-O1	2.197(13)
Co1-O1'	2.205(2)	Co1-O2	2.151(12)
Co1-O2	2.210(2)	Co1-O4	2.211(13)
Co1-O2'	2.210(2)	Co1-O5	2.229(13)
Co1-N1	2.120(2)	Co1-N1	2.189(15)
Co1-N1'	2.120(2)	Co1-N2	2.300(15)
Co1···N2	2.706(0)	Co1-N3	2.114(14)
Co1···N2'	2.706(0)	Co1···N4	3.061(0)
O1-Co1-O2	57.74(8)	O1-Co1-O2	59.50(4)
O1'-Co1-O2'	57.74(8)	O4-Co1-O5	57.97(4)
N1-Co1···N2	54.48(0)	N1-Co1-N2	60.07(5)
N1'-Co1···N2'	54.38(0)	N3-Co1···N4	48.77(0)

Table S4. The results of the continuous shape measure (CSM) analyses of **[Co(napy)$_2$(NO$_3$)$_2$]** in **1** and **2** by SHAPE software.[S31]

CSM		**1**	CSM		**1**
Six-vertex	Hexagon	20.566	Seven-vertex	Heptagon	27.690
	Pentagonal pyramid	18.603		Hexagonal pyramid	20.583
				Pentagonal bipyramid	5.010
	Octahedron	8.496		Capped octahedron	5.905
	Trigonal prism	7.428		Capped trigonal prism	4.481
	Johnson pentagonal pyramid	20.397		Johnson pentagonal bipyramid	7.981
				Johnson elongated triangular pyramid	21.071

1	CSM	Octagon	Heptagonal pyramid	Hexagonal bipyramid	Cube	Square antiprism
	Eight-vertex	34.762	22.158	15.520	10.541	5.473
	CSM	Triangular dodecahedron	Johnson gyrobifastigium	Johnson elongated triangular bipyramid	Biaugmented trigonal prism	Biaugmented trigonal
	Eight-vertex	4.880	11.101	21.988	5.080	5.547
	CSM	Snub diphenoid	Triakis tetrahedron	Elongated trigonal bipyramid		
	Eight-vertex	4.451	11.360	21.540		

CSM		**2**	CSM		**2**
Six-vertex	Hexagon	20.367	Seven-vertex	Heptagon	27.434
	Pentagonal pyramid	18.062		Hexagonal pyramid	19.905
				Pentagonal bipyramid	3.955
	Octahedron	8.829		Capped octahedron	5.047
	Trigonal prism	7.718		Capped trigonal prism	3.787
	Johnson pentagonal pyramid	19.667		Johnson pentagonal bipyramid	7.060
				Johnson elongated triangular pyramid	20.395

2	CSM	Octagon	Heptagonal pyramid	Hexagonal bipyramid	Cube	Square antiprism
	Eight-vertex	34.557	22.170	15.519	10.891	5.364
	CSM	Triangular dodecahedron	Johnson gyrobifastigium	Johnson elongated triangular bipyramid	Biaugmented trigonal prism	Biaugmented trigonal
	Eight-vertex	4.947	11.170	23.082	4.347	5.477
	CSM	Snub diphenoid	Triakis tetrahedron	Elongated trigonal bipyramid		
	Eight-vertex	4.717	10.947	22.486		

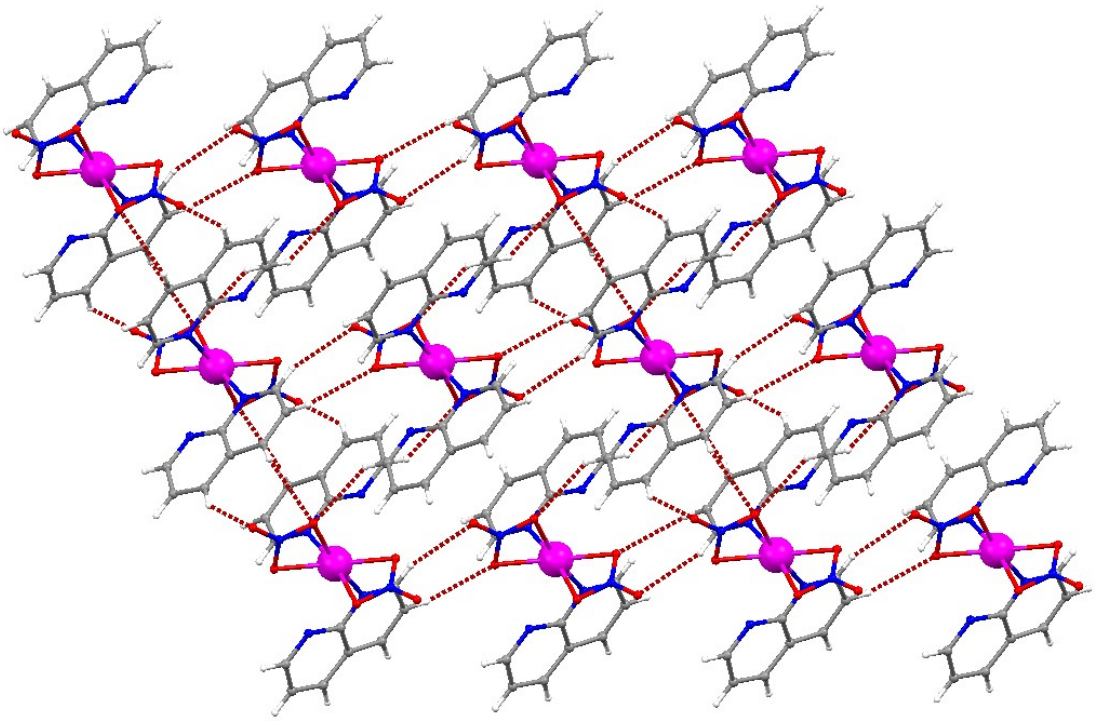

Fig. S3 The weak interactions in **1.**

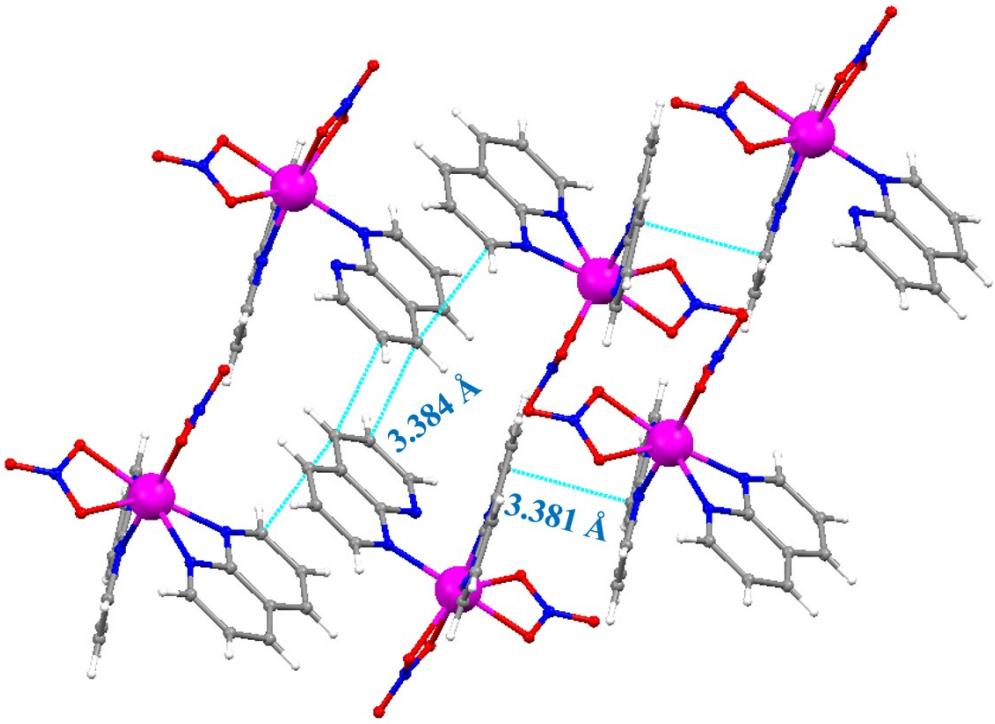

Fig. S4 The π···π stacking interactions in **2**.

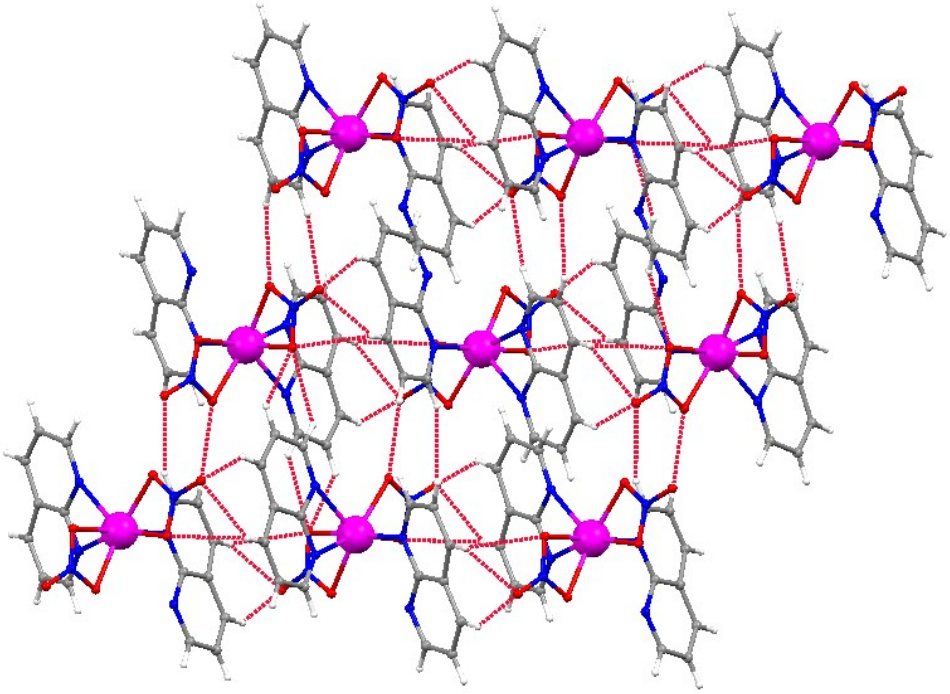

Fig. S5 Weak hydrogen bonding in **2**.

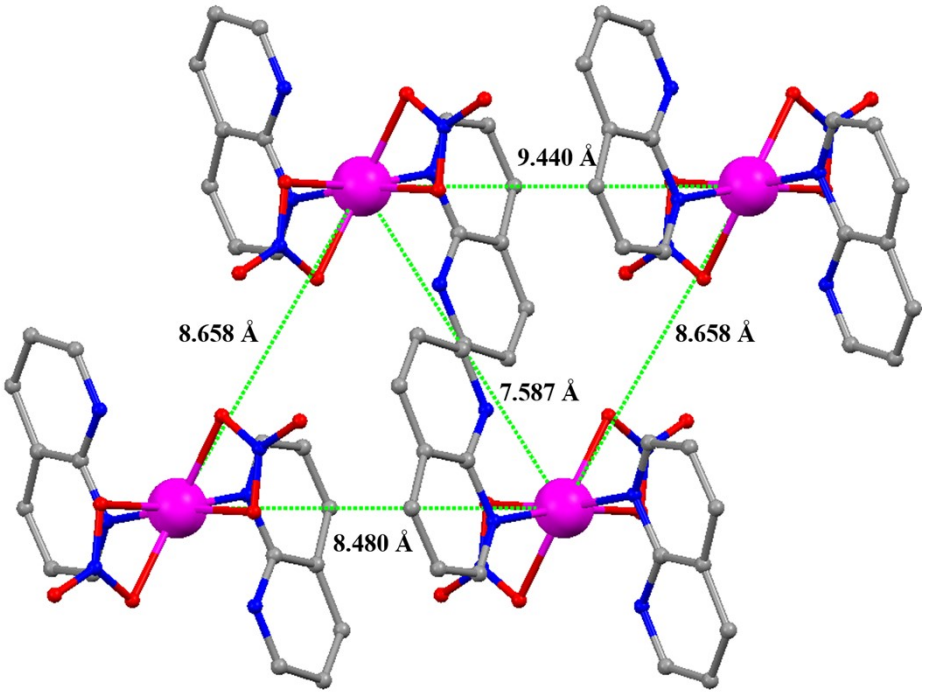

Fig. S6 The intermolecular Co-Co distances in **1.**

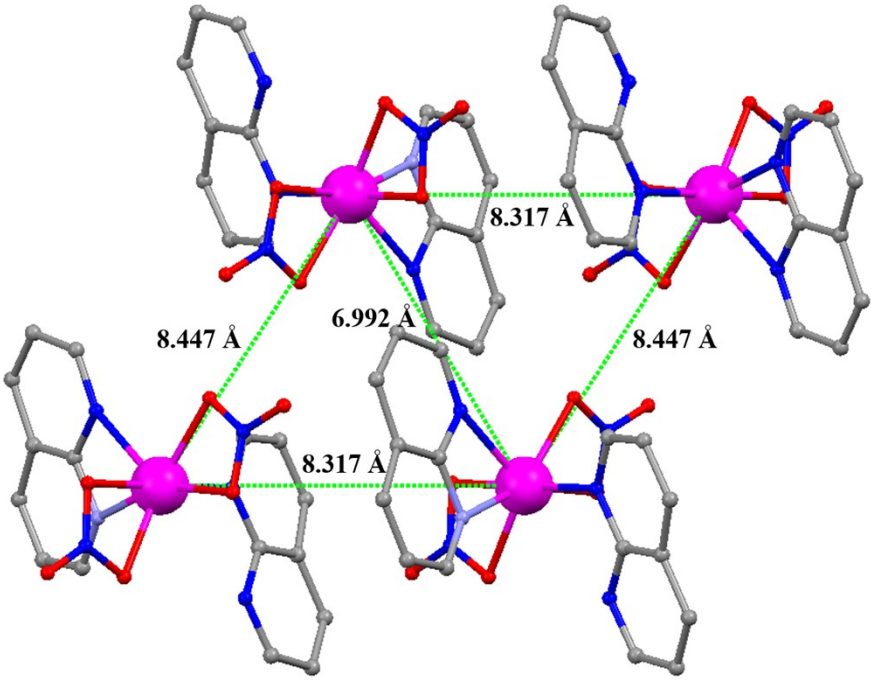

Fig. S7 The intermolecular Co-Co distances in **2.**

Table S5. Zero field splitting parameters obtained fitting the experimental data using the PHI program for **1** and **2**.

	1	**2**
D, cm^{-1}	−36.94(7)	+12.87(6)
E, cm^{-1}	+6.87(0)	+0.02(0)
g_x, g_y, g_z	2.01(6), 2.01(6), 2.41(0)	2.11(6), 2.11(6) 2.42(1)
χ_{TIP}, cm^3·K mol^{-1}	0.87(6)×10^{-3}	0.91(0)×10^{-3}
zj, cm^{-1}	−0.05(0)	-0.01(8)

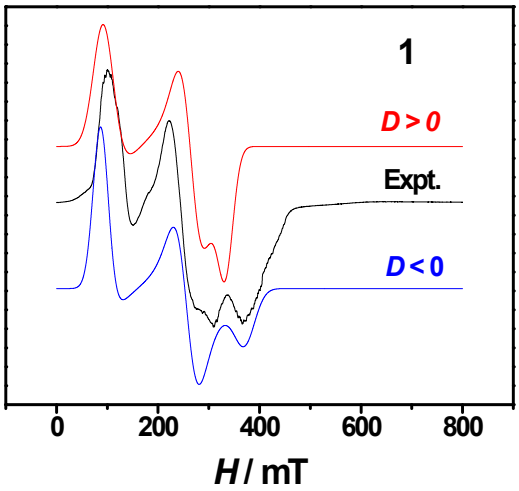

Fig. S8 Experimental X-band EPR spectrum (black) and the simulations of **1** at 2 K (red trace: positive *D* and blue trace: negative *D*).

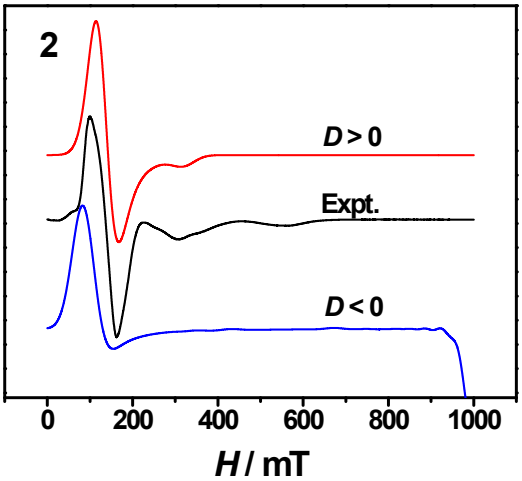

Fig. S9 Experimental X-band EPR spectrum (black) and the simulations of **2** at 2 K (red trace: positive *D* and blue trace: negative *D*).

Theoretical calculations

All theoretical calculations were pursed with the ORCA 5.0.3 package.[S32-S34] The state average complete active space self-consistent field (SA-CASSCF) was used to calculate the zero-field splitting and g-factors for Co(II)-SIMs. The CASSCF wave functions were complemented by the N-electron valence second order perturbation theory (NEVPT2) with CAS(7,5) active spaces.[S35,S36] In the state averaged approach all multiplets for the given electron configuration were equally weighted, which means 10 quartet and 40 doublet states. The ZFS parameters were calculated through

the quasi-degenerate perturbation theory (QDPT),[S37] in which approximations to the Breit-Pauli form of the spin-orbit coupling operator (RI-SOMF approximation)[S38] and the effective Hamiltonian theory were utilized.[S39] The def2-TZVP(-f) basis set S6 was used for all calculations, assisted by the autoaux basis set in the RI calculations,[S36] and the chain-of-spheres (RIJCOSX) approximation to exact exchange.[S40] Additionally, Local spin-Hamiltonian parameters g-factors have been computed by using the SINGLE_ANISO module from the EHA method.[S41]

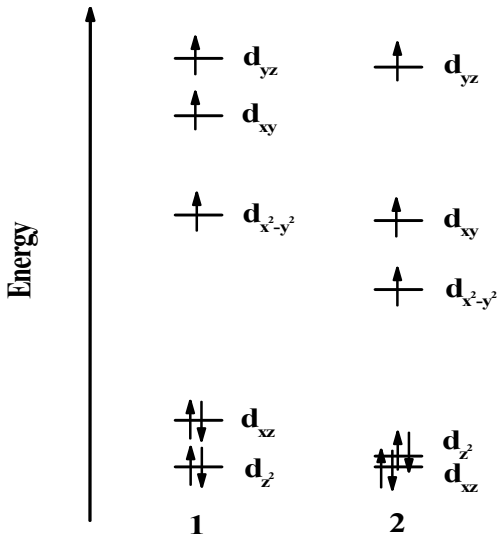

Fig. S10 Orbital energy diagrams for **1** (left) and **2** (right).

Table S6. ORCA/CASSCF+NEVPT2 computed **D**, ***E***, and g value for complex **2**.

Complex	D (cm^{-1})	E (cm^{-1})	g_{iso}	g_x	g_y	g_z
2	18.0026	5.3328	2.3149	2.1827	2.3096	2.4524

Table S7. The CASSCF/NEVPT2/def2-TZVP(-f)//def2-SVP computed Individual contributions to *D*-tensor for complex **2**.

2S+1	Root	*D*	*E*
4	0	0.000	0.000
4	1	20.206	16.431
4	2	10.269	-8.232
4	3	-19.428	0.000
4	4	5.962	-2.463
4	5	-0.018	-0.000
4	6	0.056	-0.022
4	7	0.038	-0.036
4	8	-0.000	0.000
4	9	0.035	0.035

2	0	1.524	0.000
2	1	-1.931	-0.446
2	2	0.001	-0.000
2	3	0.002	-0.000
2	4	-0.346	-0.205
2	5	-1.726	-0.890
2	6	0.093	-0.000
2	7	-1.259	0.758
2	8	4.127	-0.000
2	9	0.015	0.000
2	10	-0.299	0.221
2	11	-0.263	-0.240
2	12	-0.311	-0.260
2	13	-0.456	0.360
2	14	0.202	-0.000
2	15	-0.211	0.031
2	16	0.002	0.000
2	17	0.000	0.000
2	18	0.053	-0.000
2	19	-0.412	-0.152
2	20	1.591	0.000
2	21	0.016	0.000
2	22	-0.286	0.230
2	23	-0.234	0.233
2	24	-0.285	-0.278
2	25	-0.075	0.072
2	26	0.000	0.000
2	27	0.026	-0.000
2	28	0.091	-0.000
2	29	-0.154	-0.037
2	30	0.152	0.000
2	31	-0.079	0.009
2	32	0.010	-0.000
2	33	-0.019	0.019
2	34	-0.002	-0.000
2	35	0.001	0.000
2	36	-0.035	0.009
2	37	0.015	0.000
2	38	0.029	-0.000
2	39	-0.020	-0.019

Table S8 The optimized structure and energy of complexes **1** and **2** at the TPSS/def2-TZVP(-f) level of theory.

Complex 1

E= -75654.50762 eV

Atoms	X	Y	Z
Co	5.444504	2.794633	3.322961
O	6.560599	1.212722	2.196006
O	7.132067	1.954716	4.156401
O	8.322748	0.343817	3.212187
N	4.535419	4.130928	4.662126
N	6.632405	4.791968	5.347520
N	7.379831	1.119279	3.175613
C	3.212143	4.184435	4.772712
H	2.654712	3.603015	4.044315
C	2.543876	4.938713	5.759064
H	1.459350	4.929492	5.787399
C	3.281705	5.653831	6.673612
H	2.801467	6.232222	7.459162
C	4.693929	5.628883	6.583804
C	5.293139	4.859650	5.540396
C	7.404646	5.450141	6.195593
H	8.477077	5.373592	6.023403
C	6.919953	6.221905	7.278593
H	7.619200	6.728051	7.936669
C	5.561057	6.317635	7.466498
H	5.141608	6.906284	8.278719
O	4.328352	1.212810	4.450023
O	3.756910	1.954733	2.489593
O	2.566141	0.343964	3.433908
N	6.353561	4.130864	1.983719
N	4.256587	4.791919	1.298285
N	3.509108	1.119362	3.470428
C	7.676820	4.184391	1.873192
H	8.234227	3.602991	2.601633
C	8.345114	4.938652	0.886839
H	9.429670	4.929404	0.858498
C	7.607297	5.653764	-0.027722
H	8.087558	6.232146	-0.813278
C	6.195093	5.628808	0.062034
C	5.595869	4.859569	1.105413
C	3.484367	5.450131	0.450224
H	2.411908	5.373636	0.622433
C	3.969075	6.221912	-0.632749

H	3.269821	6.728130	-1.290781
C	5.327972	6.317609	-0.820641
H	5.747415	6.906293	-1.632803

Complex 2

E= -75655.73130 eV

Atoms	X	Y	Z
Co	5.385136	8.627277	9.819997
N	4.479266	7.290445	11.158345
N	6.577836	6.579563	11.786976
N	6.265664	7.302601	8.452747
N	4.154016	6.648416	7.806377
N	3.469075	10.318604	9.989957
N	7.333983	10.283988	9.682862
O	3.706981	9.496913	9.001852
O	4.286818	10.206458	10.965108
O	2.533275	11.101131	9.965679
O	7.08027	9.447398	10.654372
O	6.513717	10.208083	8.706359
O	8.285381	11.046917	9.722022
C	3.158558	7.261964	11.298951
H	2.595218	7.859729	10.589331
C	2.49862	6.513349	12.295076
H	1.415888	6.544784	12.349718
C	3.243298	5.774861	13.18539
H	2.770742	5.199999	13.977658
C	4.653166	5.770559	13.061087
C	5.242906	6.538229	12.010862
C	7.357404	5.895751	12.606612
H	8.426118	5.952392	12.407805
C	6.882966	5.121156	13.69224
H	7.586951	4.592227	14.32651
C	5.527522	5.053743	13.914114
H	5.116136	4.465265	14.730153
C	7.585664	7.252234	8.311411
H	8.160054	7.820331	9.036397
C	8.231426	6.51772	7.295667
H	9.314589	6.529646	7.241832
C	7.472924	5.818219	6.385809
H	7.934553	5.255989	5.57818
C	6.063206	5.837859	6.510112
C	5.48795	6.588038	7.580817
C	3.361741	6.002313	6.968554
H	2.294277	6.07354	7.169373

C	3.821512	5.249271	5.861685
H	3.107652	4.751962	5.21305
C	5.175475	5.161932	5.637745
H	5.575663	4.588446	4.805608

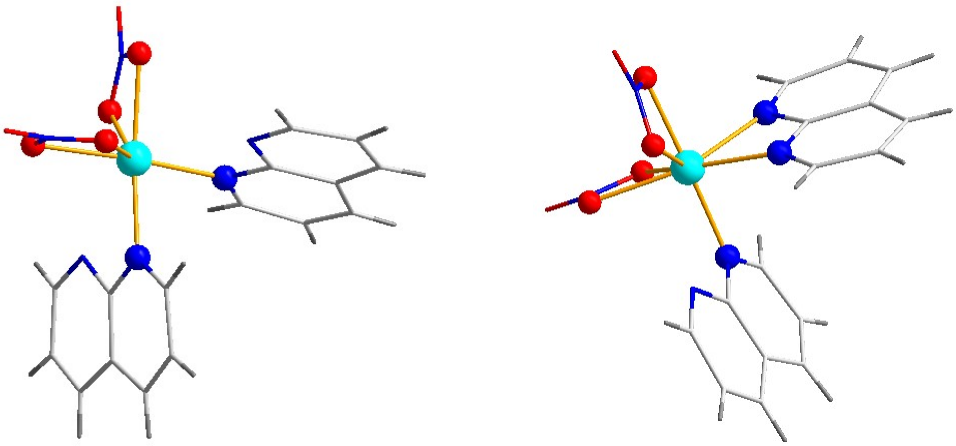

(a) Complex **1** (b) Complex **2**

Fig. S11 Calculated complete structure of complexes.

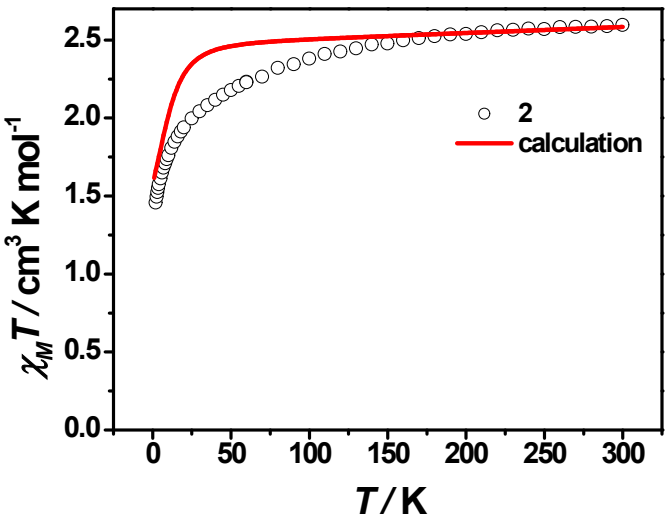

Fig. S12 Calculated (red solid line) data of magnetic susceptibilities of **2**.

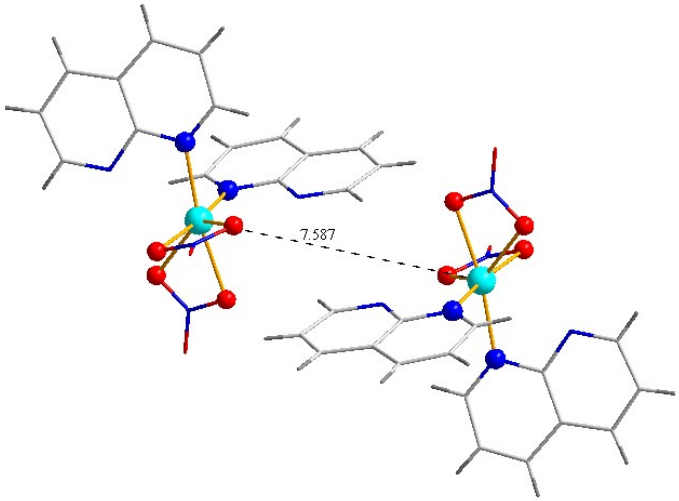

Fig. S13 The nearest fragment diagram for complex **1**.

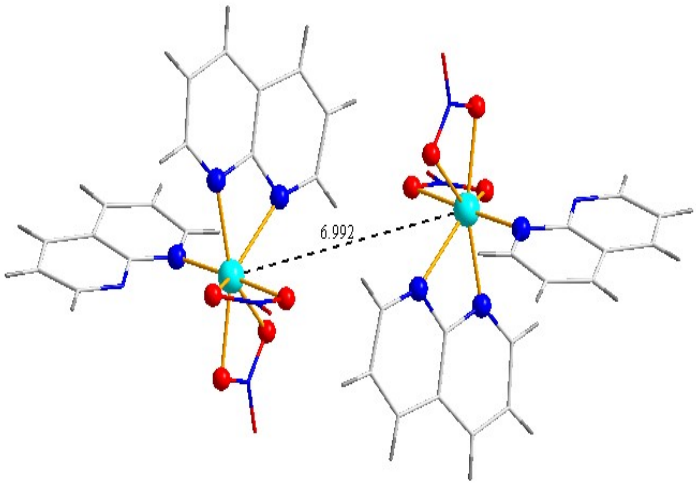

Fig. S14 The nearest fragment diagram for complex **2**.

The magnetic coupling constants were obtained by calculating the energy gap between the high spin state (E_{HS}, |+3/2,+3/2>) and the broken symmetry state (E_{BS}, |+3/2,-3/2>) at the B3LYP-D4/def2-TZVP(-f) level of theory,[S42,S43] that the density functional theory and the broken-symmetry state method (DFT-BS) was proposed by Noodleman. The magnetic coupling constant between two nearest neighbor Co-SIMs segments is can be obtained using the HDVV Hamiltonian description:

$$\hat{H} = -2J\hat{S}_1 \cdot \hat{S}_2 \qquad (2)$$

Where J is the magnetic coupling constant between Co(II) ions, and $\hat{S}_1$ and $\hat{S}_2$ are the respective spin operators representing Co(1) and Co(2) at this center.[S44]

The magnetic coupling constant between two nearest neighbor Co-SIMs segments

was evaluated using the formula proposed by Yamaguchi *et al*.[S45]

$$J = -\frac{E_{HS} - E_{BS}}{S_{\mathrm{HS}}^2 - S_{\mathrm{BS}}^2} \qquad (3)$$

where S_{HS}^2 and S_{BS}^2 represents the expectation value of the square of the spin operator for the HS state and the BS state, respectively.

Table S9. Calculated energies of HS and BS states (E_{HS} and E_{BS}) and magnetic coupling constants (J_{calc}) of complexes at the B3LYP-D4/def2-TZVP(-f) level of theory.

Co-SIMs segments	E_{HS}/eV	E_{BS}/eV	S_{HS}^2	S_{BS}^2	$J_{\mathrm{calc}}/\mathrm{cm}^{-1}$
1-the nearest distance	-151235.24904	-151235.24904	12.01669	3.01669	0.00
2-the nearest distance	-151239.20967	-151239.20967	12.01882	3.01882	0.00

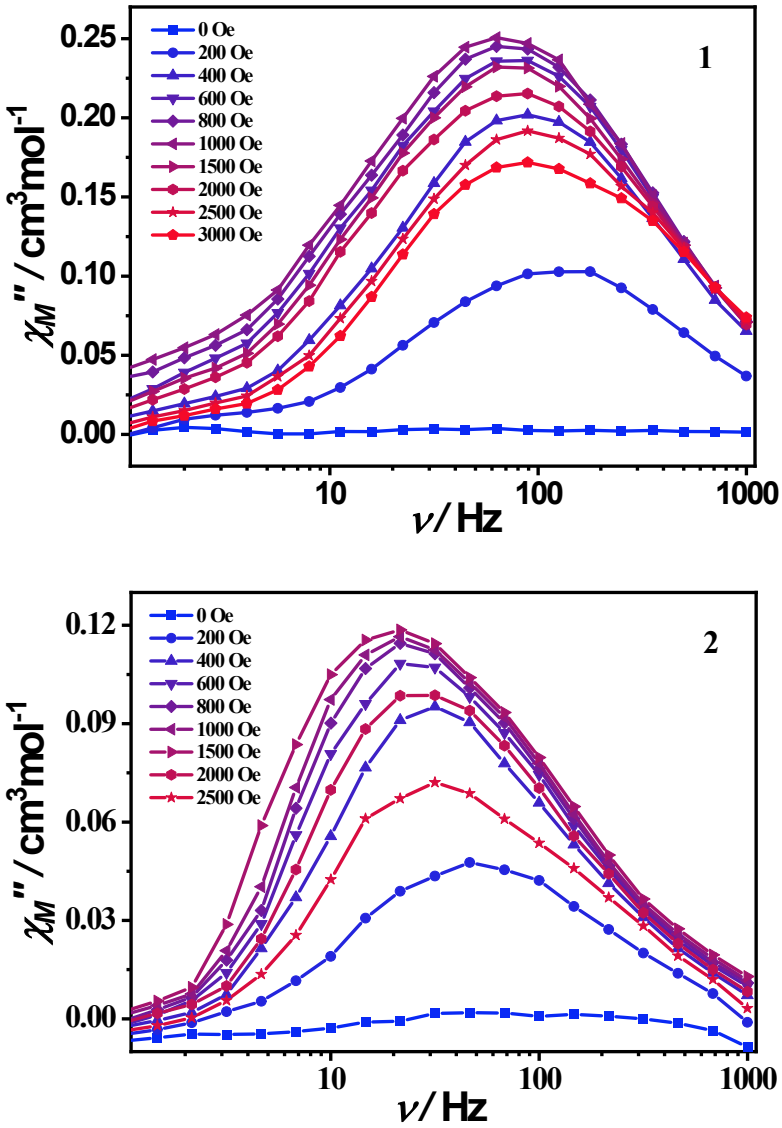

Fig. S15 Frequency dependence of out-of-phase (χ_M'') ac susceptibility at 1.8 K under the different applied static fields for **1** and **2**. The solid lines are for eye guide.

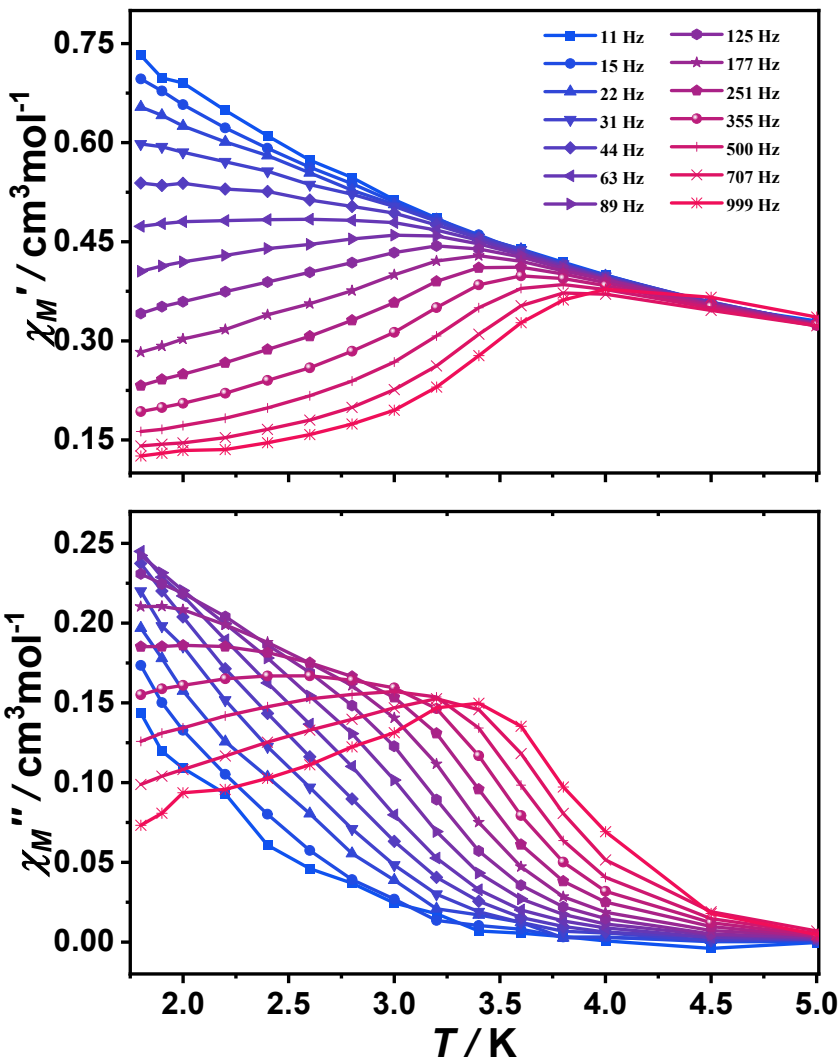

Fig. S16 Temperature dependence of in-of-phase (χ_M') and out-of-phase ac susceptibility (χ_M'') at different ac frequencies under 1000 dc field for **1**. The solid lines are for eye guide.

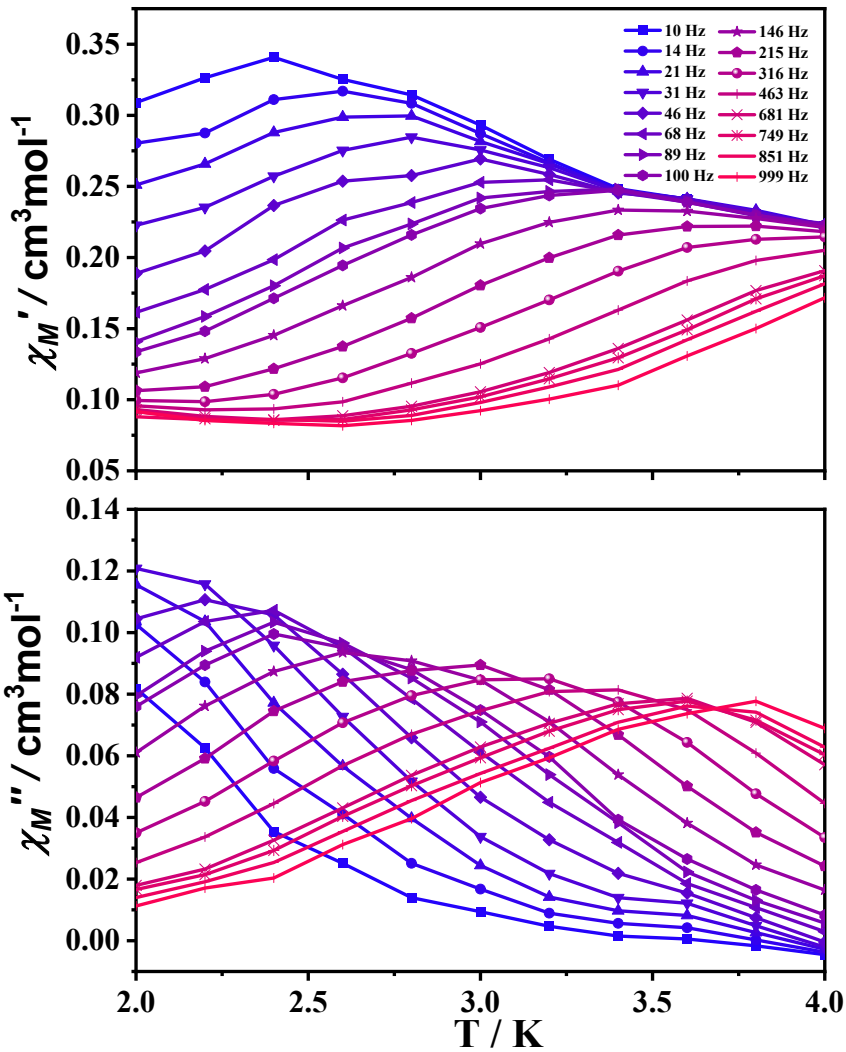

Fig. S17 Temperature dependence of in-of-phase (χ_M') and out-of-phase ac susceptibility (χ_M'') at different ac frequencies under 1500 Oe dc field for **2**. The solid lines are for eye guide.

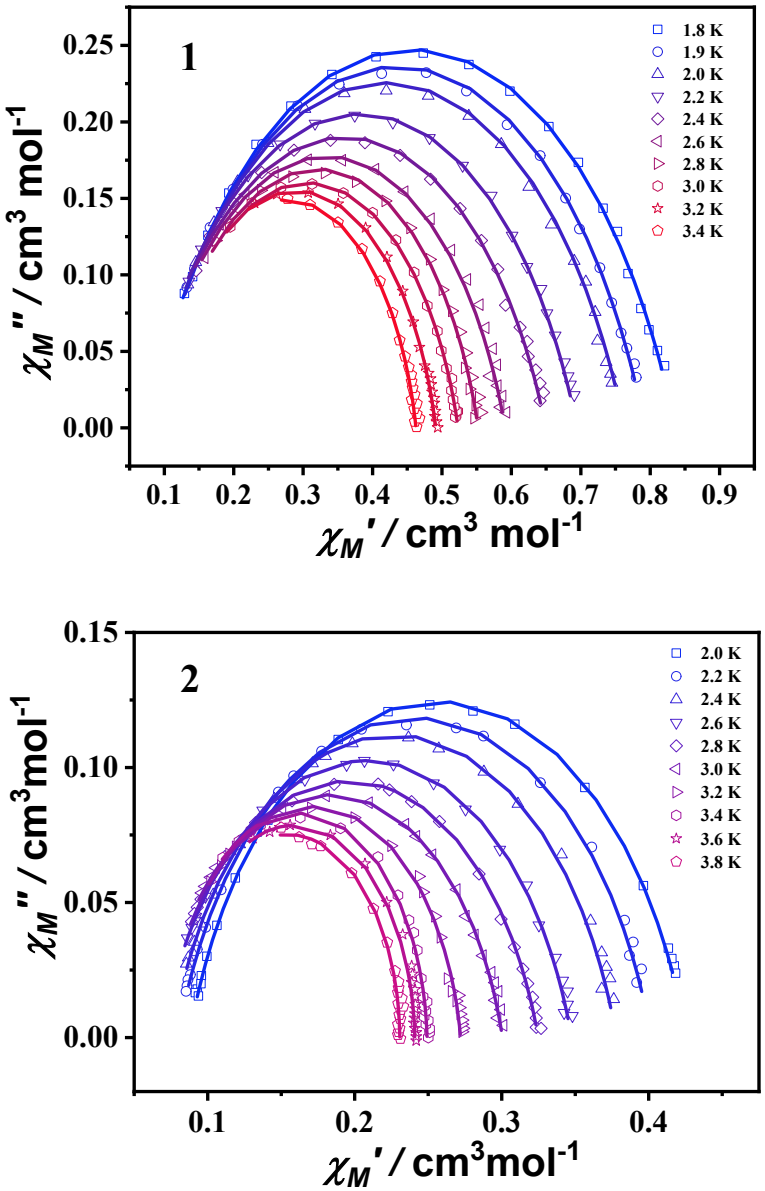

Fig. S18 Cole-Cole plot obtained from the ac susceptibility data under a different range of temperature for **1** and **2**. Solid lines represent the best fits to a generalized Debye model.[S46]

Table S10. Relaxation times τ (s) and α values for **1**.

1				
T (K)	χ_S	χ_T	τ (s)	α
1.8	0.077	0.83	0.23×10^{-2}	0.27
1.9	0.078	0.79	0.20×10^{-2}	0.26
2.0	0.074	0.76	0.18×10^{-2}	0.26
2.2	0.070	0.70	0.13×10^{-2}	0.26
2.4	0.070	0.66	0.10×10^{-2}	0.26
2.6	0.071	0.60	0.78×10^{-3}	0.25
2.8	0.076	0.56	0.58×10^{-3}	0.23
3.0	0.089	0.52	0.42×10^{-3}	0.19
3.2	0.091	0.49	0.27×10^{-3}	0.16
3.4	0.085	0.46	0.17×10^{-3}	0.15

Table S11. Relaxation times τ (s) and α values for **2**.

2				
T (K)	χ_S	χ_T	τ (s)	α
2.0	0.087	0.43	6.82×10^{-3}	0.19
2.2	0.080	0.40	4.64×10^{-3}	0.19
2.4	0.075	0.38	2.93×10^{-3}	0.19
2.6	0.069	0.35	1.80×10^{-3}	0.19
2.8	0.067	0.32	1.19×10^{-3}	0.19
3.0	0.066	0.30	7.55×10^{-4}	0.17
3.2	0.071	0.27	5.04×10^{-4}	0.10
3.4	0.075	0.25	3.36×10^{-4}	0.031
3.6	0.077	0.24	2.43×10^{-4}	0.025
3.8	0.078	0.23	1.71×10^{-4}	0.0085

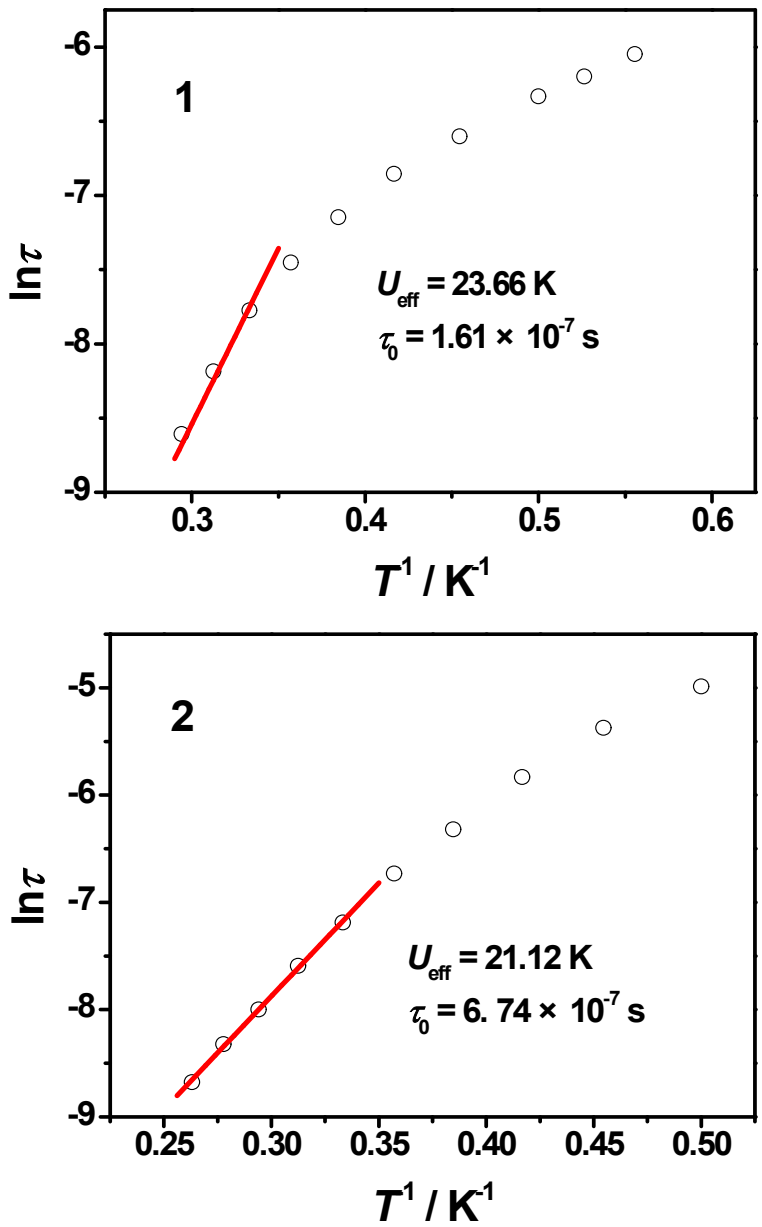

Fig. S19 Relaxation time of the magnetization *ln(τ)* vs T^{-1} plots for **1** and **2**.

At low fields, Raman process is weakly field dependent and thus they have been represented by constant of $k(T)$.[S47] In addition, both of the quantum tunneling of the magnetization and the direct processes are strongly affected by even applying a small magnetic field.[S48,S49] Therefore, the field dependence of the relaxation at 1.8 K was analyzed by eq (1),

$$\tau^{-1} = AH^4T + \frac{B_1}{1+B_2H^2} + k(T) \tag{1}$$

where the first term represents direct process, the second term represents quantum tunneling of magnetization and the last term represents Raman processes.

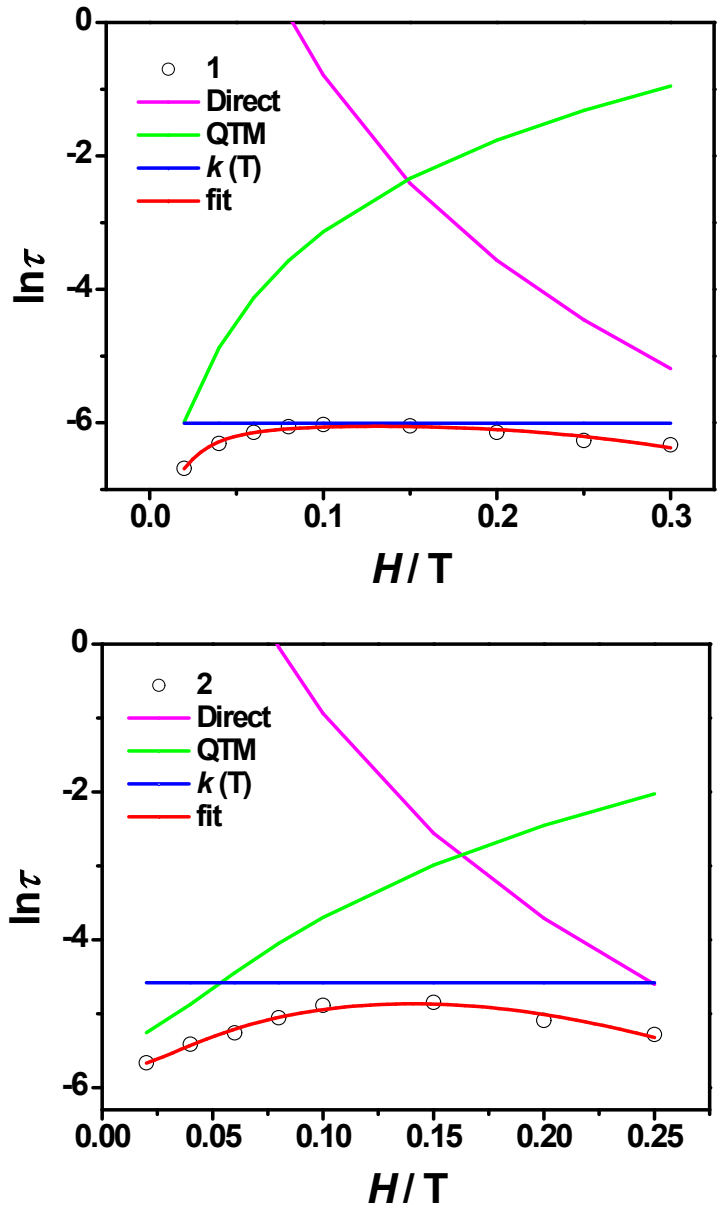

Fig. S20 Field dependence of the magnetization relaxation rates for **1** under 1.8 K and **2** under 2 K. The red line represents the best fit by using eq (1). The other lines represent the contribution of direct (purple), QTM (green) and Raman processes (blue), respectively.

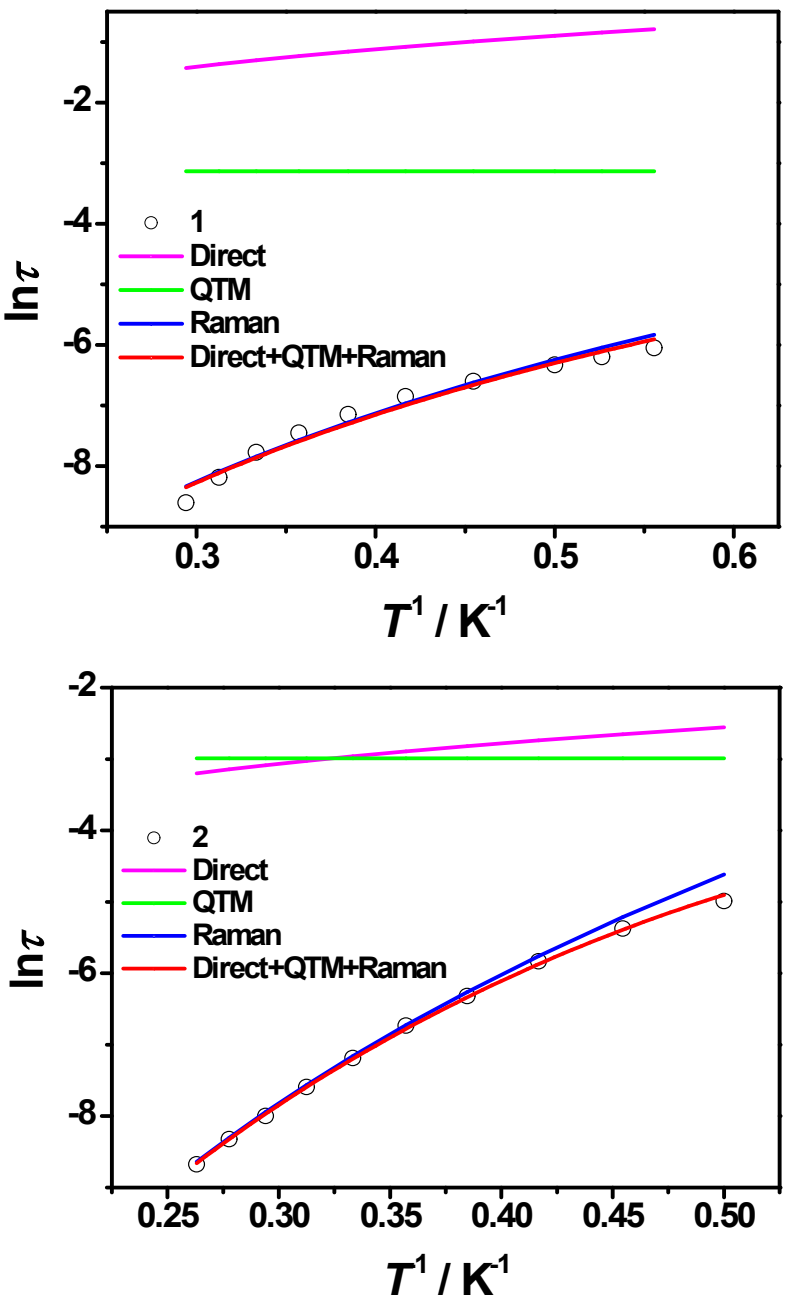

Fig. S21 Temperature dependence of the magnetization relaxation rates for **1** and **2**. The red line represents the best fit by a model including three possible relaxation processes. The other lines represent the contribution of direct (purple), QTM (green) and Raman processes (blue), respectively.

References

S1 Wu, D. Y.; Zhang, X. X.; Huang, P.; Huang, W.; Ruan, M. Y.; Ouyang, Z. W. *Inorg. Chem.,* **2013**, *52*, 10976-10982.

S2 Xie, Q.-W.; Wu, S.-Q.; Shi, W.-B.; Liu, C.-M.; Cui, A.-L.; Kou, H.-Z. *Dalton Trans.,* **2014**, *43*, 11309-11316.

S3 Díaz-Torres, R.; Menelaou, M.; Roubeau, O.; Sorrenti, A.; Brandariz-de-Pedro, G.; Saňudo, E. C.; Teat, S. J.; Fraxedas, J.; Ruiz, E.; Aliaga-Alcalde, N. *Chem. Sci.,* **2016**, *7*, 2793-2803.

S4 Roy, S.; Oyarzabal, I.; Vallejo, J.; Cano, J.; Colacio, E.; Bauza, A.; Frontera, A.; Kirillov, A. M.; Drew, M. G. B.; Das, S. *Inorg. Chem.,* **2016**, *55*, 8502-8513.

S5 Walsh, J. P. S.; Bowling, G.; Ariciu, A.-M.; Jailani, N. F. M.; Chilton, N. F.; Waddell, P. G.; Collison, D.; Tuna, F.; Higham, L. J.; *Magnetochem.,* **2016**, *2*, 23 (1-10).

S6 Valigura, D.; Rajnák, C.; Moncol, J.; Titiš, J.; Boča, R. *Dalton Trans.,* **2017**, *46*, 10950-10956.

S7 Boča, R.; Rajnák, C.; Moncol, J.; Titiš, J.; Valigura, D. *Inorg. Chem., 2018*, *57*, 14314-14321.

S8 Wei, Y.-F.; Ma, X.-F.; Huang, X.-D.; Wen, G.-H.; Jia, J.-G.; Zheng, L.-M. *J. Solid State Chem.,* **2022**, *312*, 123227.

S9 Nemec, I.; Fellner, O. F.; Indruchová, B.; Herchel, R. *Materials,* **2022**, *15*, 1064.

S10 Xia, Z.; Li, Y.; Ji, C.; Jiang, Y.; Ma, C.; Gao, J.; Zhang, J. *Nanomaterials*, **2022**, *12*, 707(1-8).

S11 Novitchi, G.; Jiang, S. D.; Shova, S.; Rida, F.; Hlavička, I.; Orlita, M.; Wernsdorfer, W.; Hamze, R.; Martins, C.; Suaud, N.; Guihéry, N.; Barra, A.-L.; Train, C. *Inorg. Chem.,* **2017**, *56*, 14809-14822.

S12 Acharya, A.; Swain, A.; Chakraborty, V.; Kumar, P.; Kumar, J.; Gonzalez, F.; Cador, O.; Pointillart, F.; Rajaraman, G.; Chandrasekhar, V. *Inorg. Chem.,* **2019**, *58*, 10725-10735.

S13 El-Ghayoury, O. A.; Lloret, F.; Julve, M.; Avarvari, N. *Eur. J. Inorg. Chem.,* **2018**, *3-4*, 449-457.

S14 Rajnák, C.; Titiš, J.; Moncol, J.; Boča, R. *Dalton Trans.,* **2020**, *49*, 4206-4210.

S15 Huang, X.-C.; Li, J.-X.; Chen, Y.-Z.; Wang, W.-Y.; Xu, R.; Tao, J.-X.; Shao, D.; Zhang, Y.-Q. *Chem Asian J.,* **2020**, *15*, 1469-1477.

S16 Zhang, Y.-J.; Yin, L.; Li, J.; Hu, Z.-B.; Ouyang, Z.-W.; Song, Y.; Wang, Z. *RSC Adv.,* **2020**, *10*, 12833-12840.

S17 Sadhukhan, D.; Ghosh, P.; Gómez-García, C. J.; Rouzieres, M. *Magnetochemistry,* **2018**, *4*, 56.

S18 Wu, Y.-W.; Tian, D.-N; Ferrando-Soria, J.; Cano, J.; Yin, L.; Ouyang, Z.-W; Wang, Z.-X; Luo, S.-C; Liu X.-Y; Pardo, E. *Inorg. Chem. Front.,* **2019**, *6*, 848-856.

S19 Hu, Z.-B.; Jing, Z.-Y.; Li, M.-M.; Yin, L.; Gao, Y.-D.; Yu, F.; Hu, T.-P.; Wang, Z.; Song, Y. *Inorg. Chem.,* **2018**, *57*, 10761-10767.

S20 Huang, X.-C.; Zhou, C.; Shao, D. Wang, X.-Y. *Inorg. Chem.,* **2014**, *53*, 12671-12673.

S21 Habib, F.; Korobkov, I.; Murugesu, M. *Dalton Trans.,* **2015**, *44*, 6368-6373.

S22 Ruamps, R.; Batchelor, L. J.; Maurice, R.; Gogoi, N.; Jiménez-Lozano, P.; Guihéry, N.; de Graaf, C.; Barra, A.-L.; Sutter , J.-P.; Mallah, T. Chem. Eur. J. 2013, 19, 950-956.

S23 Chen, L.; Chen, S.-Y.; Sun, Y.-C.; Guo, Y.-M.; Yu, L.; Chen, X.-T.; Wang, Z.; Ouyang, Z. W.; Song, Y.; Xue, Z.-L. *Dalton Trans.,* **2015**, *44*, 11482-11490.

S24 Huang, X.-C.; Qi, Z.-Y.; Ji, C.-L.; Guo, Y.-M.; Yan, S.-C.; Zhang, Y.-Q.; Shao, D.; Wang, X.-Y. *Dalton Trans.,* **2018**, *47*, 8940-8948.

S25 Wang, J.; Cui, H.-H.; Zhang, Y.-Q.; Chen, Lei.; Chen, X.-T. *Polyhedron,* **2018**, *154*, 148-155.

S26 Mondal, A. K.; Mondal, A.; Dey, B.; Konar, S. *Inorg. Chem.,* **2018**, *57*, 9999-10008.

S27 Antal, P.; Drahoš, B.; Herchel, R.; Trávníček, Z. *Eur. J. Inorg. Chem.* **2018**, *38*, 4286-4297.

S28 Kopotkov, V. A.; Korchagin, D. V.; Sasnovskaya, V. D.; Gilmutdinov, I. F.; Yagubskii, E. B. *Magnetochemistry,* **2019**, *5*, 58(1-16).

S29 Mondal, A.; Kharwar, A. K.; Konar, S. *Inorg. Chem.,* **2019**, *58*, 10686-10693.

S30 Uchida, K.; Cosquer, G.; Sugisaki, K.; Matsuoka, H.; Sato, K.; Breedlove B. K.; Yamashita, M. *Dalton Trans.,* **2019**, *48*, 12023-12030.

S31 Llunell, M.; Casanova, D.; Cirera, J.; Alemany, P.; Alvarez, S. Shape Program,

Version 2.1, **2013**.

S32 Neese, F. *Wiley Interdiscip. Rev.: Comput. Mol. Sci.* **2012**, *2*, 73-78.

S33 Neese, F. Software update: The ORCA program system—Version 5.0, WIREs *Comput. Mol. Sci.* **2022**, *12*, e1606.

S34 Neese, F. ORCA-an Ab Initio, Density functional and semiempirical program package, 5.0.3, University of Bonn, Bonn, Germany, **2022**.

S35 Malmqvist, P. A.; Roos, B. O. *Chem. Phys. Lett.* **1989**, *155*, 189-194.

S36 Herchel, R.; Nemec, I.; Machata, M.; Trávníček, Z. *Dalton Trans.* **2016**, *45*, 18622-18634.

S37 Ganyushin, D.; Neese, F. *J. Chem. Phys.* **2006**, *125*, 024103.

S38 Neese, F. *J. Chem. Phys.* **2005**, *122*, 034107.

S39 Weigend, F.; Ahlrichs, R. *Phys. Chem. Chem. Phys.* **2005**, *7*, 3297-3305.

S40 Weigend, F. *Phys. Chem. Chem. Phys.* **2006**, *8*, 1057-1065.

S41 Zhou, Y.; Tan, P.; Jing, R.; Liu, M.; Xiang, Y.; Yuan, A.; Luo, S.-C.; Cui, H.-H.; Shi, L.; Chen, L. *Cryst. Growth Des.* **2022**, *22*, 6792-6800.

S42 Noodleman, L. *J. Chem. Phys.* **1981**, 74, 5737-5743.

S43 Luo, S.; Nie, D.; Li, Z.; Sun, X.; Hu, L.; Liu, X. *Polyhedron* **2020**, *182*, 114506.

S44 Luo, S.; Mei, H.; Sun, X.; Zheng, P. *J. Mol. Graph. Model.* **2020**, *97*, 107562.

S45 Soda, T.; Kitagawa, Y.; Onishi, T.; Takano, Y.; Shigeta, Y.; Nagao, H.; Yoshioka, Y.; Yamaguchi, K. *Chem. Phys. Lett.* **2000**, *319*, 223-230.

S46 Cole, K. S.; Cole, R. H. *J. Chem. Phys.* **1941**, *9*, 341-351.

S47 Shrivastava, K. N. *Phys. Status Solidi B* **1983**, *117*, 437-458.

S48 Abragam, A.; Bleaney, B. Electron paramagnetic resonance of transition ions, Dover, New York, **1986**.

S49 Lucaccini, E.; Sorace, L.; Perfetti, M.; Costes, J.-P.; Sessoli, R. *Chem. Commun.* **2014**, *50*, 1648-1651.